Physics of the Earth and Planetary Interiors 354 (2024) 107225

Contents lists available at ScienceDirect

Physics of the Earth and Planetary Interiors

journal homepage: www.elsevier.com/locate/pepi

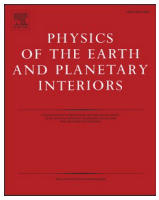

Thermal instability from rock magnetic measurements confirms the underestimates of absolute paleointensity records during the Santa Rosa geomagnetic excursion

Junxiang Miao [a,b], Huapei Wang [b,*]

[a] School of Earth Sciences, China University of Geosciences, Wuhan, Hubei 430074, China
[b] Paleomagnetism and Planetary Magnetism Laboratory, School of Geophysics and Geomatics, China University of Geosciences, Wuhan, Hubei 430074, China

ARTICLE INFO

Keywords:
Rock magnetic measurements
Paleointensity
Santa Rosa geomagnetic excursion
Thermal instability
Hysteresis properties
Earth's magnetic field

ABSTRACT

Geomagnetic excursion events have been widely studied in recent years as a key process for understanding the evolution of the Earth's magnetic field. The Santa Rosa geomagnetic excursion (SRE) event during the Matuyama chron has been globally recorded in sediment sequences and lava flows. Galapagos lavas distributed in near-equatorial with an $^{40}Ar/^{39}Ar$ age of 925.7 ± 4.6 ka display absolute paleointensity values of about 14% of the modern magnetic field, which is a valuable record of the Earth's magnetic field strength during the SRE event. However, the above extremely low estimates of paleointensities during the SRE were fitting from higher temperature segments (400 °C–575 °C) from previous paleointensity experiments, which is biased by the thermal instability of Galapagos lava samples during high-temperature heating treatments. From our comprehensive rock magnetic experiments in this study, Galapagos lava samples exhibit thermal instability after heating treatments higher than 400 °C. The severe thermal alteration occurred after the heating temperature reached 500 °C, mainly manifested as an increase in remanence-carrying capacities, such as the enhanced ability of paleointensity specimens to record partial thermoremanent magnetization, resulting in underestimated paleointensities during the SRE. In-depth experiments on rock magnetism and hysteresis parameters analysis provide a powerful method to detect the thermal instability of lava samples, which can help us confirm the biased geomagnetic field strength during this short-lived excursion period and prevent misinterpretations of the Earth's magnetic field evolution through erroneous low paleointensity records.

1. Introduction

Geomagnetic excursions provide important observations of how Earth's magnetic field has evolved (Singer et al., 1999; Singer, 2014; Balbas et al., 2016; Channell, 2017; Simon et al., 2018). Precise chronologies from marine sediment sequences are the main tool used to identify magnetic excursion events, which occur throughout the geological record (Channell et al., 2002; Horng et al., 2002; Singer, 2014; Simon et al., 2018). Moreover, much recent research has focused on obtaining accurate paleointensity records to reveal further details of the mechanisms behind these geomagnetic instabilities and deepen our understanding of core dynamo behavior (Moskowitz et al., 1993; de Groot et al., 2015; Wang et al., 2015; Bono et al., 2019; Zhou et al., 2022).

The Santa Rosa excursion (SRE) event was initially identified in the Santa Rosa I rhyolite dome in Valles Caldera, New Mexico (USA) (Doell and Dalrymple, 1966), with a $^{40}Ar/^{39}Ar$ age of 932 ka obtained from geochronologic studies (Singer, 2014). Horng et al. (2002) established a high-quality magnetostratigraphic and oxygen isotope record from sediments in the western Philippine Sea during the Matuyama Chron and estimated a calibrated age of 920–925 ka for the SRE interval. The SRE event was also recorded in sediment cores at Ocean Drilling Program (ODP) Sites 983 and 984 in the Iceland Basin (Channell et al., 2002). Low paleointensity estimates (4.23 ± 1.29 μT) and intermediate virtual geomagnetic poles (VGPs) in samples from the Galapagos GA-X site (Kent et al., 2010; Wang and Kent, 2013, 2021) helped Balbas et al. (2016) identify a low-latitude record of the SRE with a new $^{40}Ar/^{39}Ar$ age of 925.7 ± 4.6 ka for basaltic lava samples from Floreana Island in the Galapagos Archipelago.

As a significant geomagnetic excursion, the SRE demonstrates the

* Corresponding author at: School of Geophysics and Geomatics, China University of Geosciences, Wuhan, Hubei, China.
E-mail address: huapei@cug.edu.cn (H. Wang).

https://doi.org/10.1016/j.pepi.2024.107225
Received 15 March 2024; Received in revised form 27 June 2024; Accepted 27 June 2024
Available online 28 June 2024
0031-9201/© 2024 Elsevier B.V. All rights are reserved, including those for text and data mining, AI training, and similar technologies.

millennium-scale instability of the geomagnetic field. However, its short-lived timespan limits the ability to widely record and recognize this event in global lava sequences (Channell et al., 2002; Balbas et al., 2016; Channell, 2017). Channell et al. (2002) provide a short interval of about 3 kyr during the SRE event based on the higher sediment rates of ODP cores from the Iceland Basin. Therefore, samples from the Galapagos GA-X site were the rare recorders that provided the magnetic field strength during the SRE, which is extremely valuable for understanding the mechanism of the SRE event and geomagnetic field evolution.

Thellier-series paleointensity experiments are among the most reliable methods for deriving absolute paleointensities (Thellier and Thellier, 1959; Coe, 1967b; Yu and Tauxe, 2005; Wang and Kent, 2013, 2021) and are widely used in studies of the paleomagnetic field. However, thermally-induced physical and chemical alteration of lava samples during stepwise heating in Thellier-series experiments (Thellier and Thellier, 1959) can compromise the fidelity of paleointensity estimates (Coe, 1967a; Thomas, 1993; Kosterov and Pre vot, 1998; Smirnov and Tarduno, 2003; Carvallo et al., 2006; Qin et al., 2011; de Groot et al., 2014a; Kim et al., 2018; Grappone et al., 2021; Wang and Kent, 2021; Jeong et al., 2021; Tema et al., 2022; Hawkins et al., 2023). Moreover, conventional methods to detect thermal alteration, such as the widely used partial thermoremanent magnetization (pTRM) check, has its inherent weakness (Coe, 1967a; Qin et al., 2011; Wang and Kent, 2013, 2021; Zhao et al., 2014). Coe (1967a) first noted that passing the pTRM check does not ensure the absence of thermal changes in a sample because it only detects thermal alteration in magnetic particles with blocking temperatures below the check temperature, potentially concealing the effect of thermal alteration in paleointensity estimates, even when pTRM check passed.

Based on the Thellier-series paleointensity experiments, Wang and Kent (2013, 2021) developed the Repeat thEllier-Series ExperimenT (RESET) paleointensity method to further analyze the thermal stability of measured samples and correct the multidomain (MD) effect during paleointensity experiments. Galapagos lava samples provide an average paleointensity of 4.23 1.29 T fitting by 400 C 575 C segments in the previous RESET paleointensity method. However, an investigation of room-temperature hysteresis behavior in a Galapagos sister specimen (GA 84.6y) displayed thermal instability during heating steps above 500 C, which was not apparent in the pTRM checks (Wang and Kent, 2021). Moreover, paleointensity estimates from GA-X samples were derived from linear regressions of high-temperature intervals (400 C 575 C) in Arai diagrams. This may have caused the previous paleointensity estimates for the SRE interval to remain biased by the thermal instability of Galapagos lavas, which is a serious risk to understanding the instability of the Earth s magnetic field during excursion events based on erroneous absolute paleointensity records.

The above discussions promote us to evaluate the thermal stability of critical lava samples in the Galapagos GA-X site used in previous paleointensity studies (Wang and Kent, 2013, 2021) through comprehensive rock magnetic experiments to confirm the reliability of paleointensities from the Santa Rosa geomagnetic excursion. We utilized room-temperature rock magnetic measurements after multiple heating-cooling treatments at critical temperatures (400 C and 500 C) for paleointensity estimates to track thermal alteration in the GA-X site specimens and assess their thermal stability. We also utilized high-temperature thermal fluctuation tomography (HT-TFT) for selected GA-X specimens to characterize their thermal alteration behavior during heating from room temperature to Curie temperatures. Building on previous studies, we detected the thermal instability of Galapagos lava samples and confirmed the underestimates in existing paleointensity records from previous studies. This critical information can help us prevent misunderstandings of geomagnetic field behavior during the short-lived excursion interval and Earth s magnetic field evolution from erroneous low paleointensities.

2. Materials and methods

The Galapagos lava samples in the GA-X site (mean Decl 212.7 ; mean Incl 26.5 ; A95 5.0) from Floreana Island in the near-equatorial Galapagos Archipelago were collected by Rochette et al. (1997) (Fig. 1). Each 25-mm-diameter cylindrical GA-X sample was cut into three specimens (Wang and Kent, 2013). Specimens labeled x were 10-mm-diameter cylinders drilled from the center part of each sample for future studies (Wang and Kent, 2013). To ensure internal consistency, a 10-mm-diameter half-cylinder from the edge of each sample was crushed into sister specimens (i , s , t , u , v , w specimens, etc.) for use in rock magnetic experiments (Wang and Kent, 2013). The remaining 25-mm-diameter cylinder, labeled c , and the GA-Xc specimens were used in previous paleointensity experiments (Wang and Kent, 2013, 2021). Referring to the rock magnetic results by Wang and Kent (2013), the magnetic carrier within the Galapagos lavas is titanomagnetite with non-single-domain (non-SD) magnetic behavior.

A fresh ~20 mg chip (referred to as v specimens) selected from each rock magnetic specimen (GA 78.2v, GA 78.5v, GA 79.1v, GA 79.4v, GA 84.1v, GA 85.1v, and GA 85.7v) was used for low-temperature thermal fluctuation tomography (LT-TFT) to assess the properties and grain size of fine magnetite particles in the Galapagos lavas. Measurements were conducted on a vibrating sample magnetometer (VSM) from PMC equipped with a low-temperature cryostat in the Institute for Rock Magnetism, University of Minnesota. Hysteresis loops and back-field direct current demagnetization (DCD) curves were measured at cryogenic temperatures from 20 K to 320 K in 10 K increments on v specimens. We also obtained field-cooled and zero-field-cooled (FC ZFC) remanence warming curves (Moskowitz et al., 1993) as well as low-temperature demagnetization (LTD) cooling and warming curves of room temperature saturation isothermal remanence ($SIRM_{RT}$) at 5 K intervals from 10 K to 300 K on u specimens (GA 78.2u, GA 78.5u, GA 79.1u, GA 79.4u, GA 84.1u, GA 84.6u, GA 85.1u, and GA 85.7u), using a Quantum Designs magnetic properties measuring system (MPMS) at the Institute for Rock Magnetism, University of Minnesota. In addition, back-scattered electron (BSE) imaging was conducted on another selected specimen, GA 84.6u, to further identify the composition and size distribution of magnetic carrier minerals within GA-X specimens. The above BSE imaging was conducted by an electron probe micro-analyzer at Wuhan Sample Solution Analytical Technology Co., Ltd., Wuhan, China. The analysis used the JXA-8230 model from JEOL with a 1 m beam diameter and either 15 kV or 20 kV accelerating voltage.

We selected sister specimens i from 10 Galapagos rock magnetic specimens, including two from GA 78 (GA 78.2i and GA 78.8i), three from GA 79 (GA 79.4i, GA 79.5i, and GA 79.8i), three from GA 84 (GA 84.1i, GA 84.3i, and GA 84.6i), and two from GA 85 (GA 85.2i and GA 85.3i) to evaluate the thermal stability in each. Target temperatures of 400 C and 500 C were chosen for our multi-cycle measurements because similar temperature intervals (400 C 575 C) were used for paleointensity estimates from the Arai diagrams of GA-Xc specimens (Wang and Kent, 2013). The measurement procedure consists of five steps: 1. rock magnetic measurements on fresh specimens; 2. heat specimens to 400 C followed by cooling to room temperature to measure rock magnetic curves; 3. repeat the heating-cooling cycle to a target temperature of 400 C three times, then measure rock magnetic curves at room temperature; 4. heat specimens to 500 C followed by cooling to room temperature to measure rock magnetic curves; 5. repeat the heating-cooling cycle to a target temperature of 500 C three times, then measure rock magnetic curves at room temperature. The entire set of measurements for each specimen included eight heating-cooling cycles.

Ten GA-Xi chips were heated to the critical target temperatures (400 C and 500 C) in an ASC TD-48 oven. After each heating-cooling cycle, hysteresis loops, isothermal remanent magnetization (IRM) acquisition curves, DCD curves, and first-order reversal curves (FORCs) were measured using an alternating gradient force magnetometer (AGFM) at the Rutgers Paleomagnetic Laboratory. A maximum field of 1

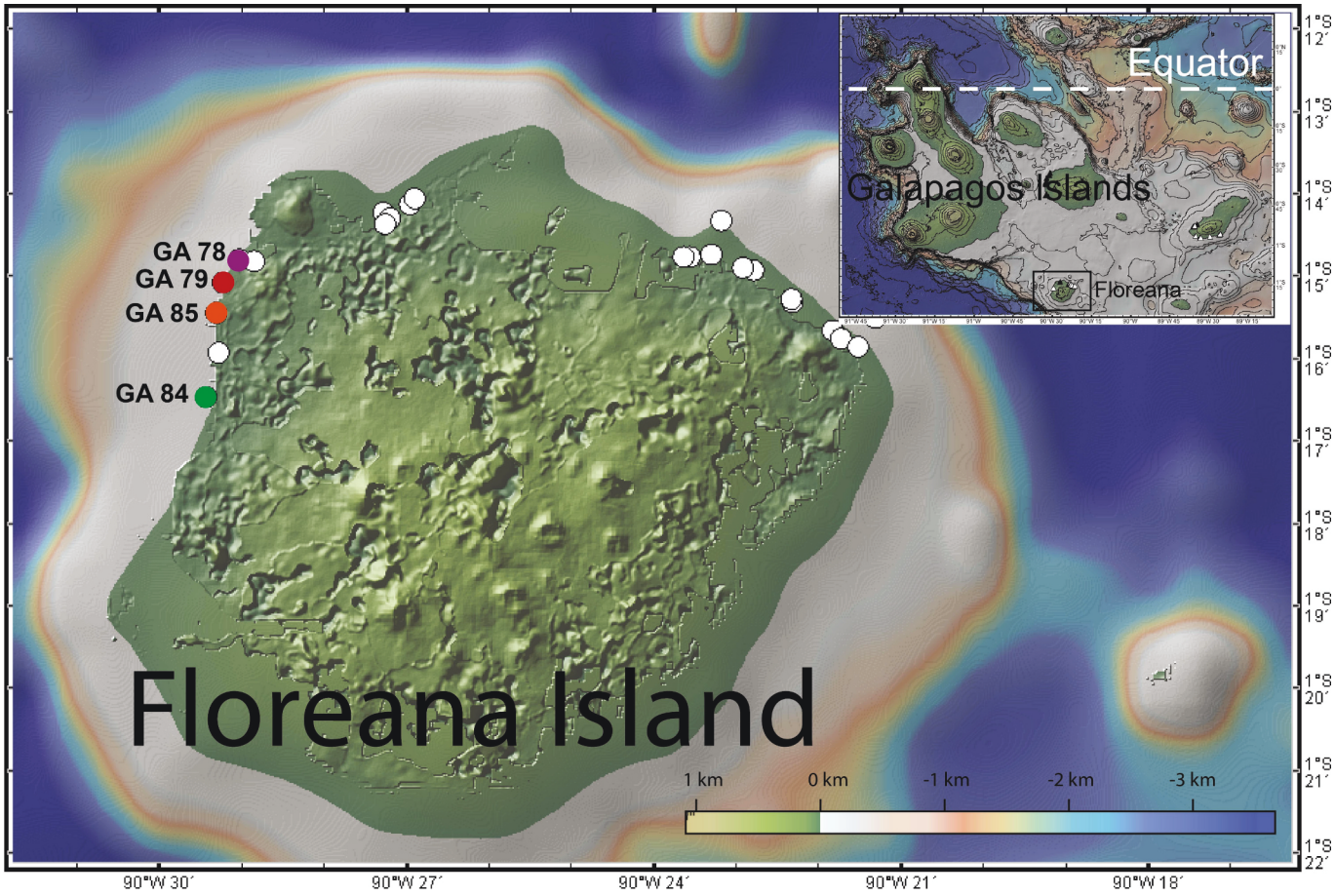

Fig. 1. Location map of the GA-X site (GA 78, GA 79, GA 84, and GA 85) from Floreana Island in the Galapagos Archipelago. Figures and captions are modified by Wang and Kent (2013) and Wang et al. (2015). White dots are sampling sites from previous studies of Rochette et al. (1997) and Kent et al. (2010) that are not discussed in this paper.

T was applied in all rock magnetic measurements. We also extracted M_s (saturation magnetization), M_{rs} (remanent magnetization), and B_c (magnetic coercivity) after applying a linear high-field correction above 70% to hysteresis loops, while B_{cr} (remanent coercivity) was calibrated from the DCD curves. To constrain the composition of various magnetic carriers within GA-X samples, we chose to decompose the measured IRM acquisition curves using the MAX UnMix web application (Maxbauer et al., 2016) to analyze the coercivity components of the GA-Xi specimens.

To gain insight into the thermophysicochemical alteration characteristics following specimen heating to near-Curie temperatures, we conducted high-temperature thermal fluctuation tomography (HT-TFT) experiments (Jackson et al., 2006). These were performed on fresh ~20 mg chips from four half-cylinders, including GA 78.5, GA 79.1, GA 84.1, and GA 85.1, to assess the thermal stability of these specimens after heating to near the Curie temperatures. We labeled these specimens "w" and used a helium gas atmosphere in all high-temperature VSM measurements. Rock magnetic curves (hysteresis loops and DCD curves) were measured during heating from room temperature to 607 °C in 20 °C increments. No data was collected during cooling. We then repeated measurements over the entire room temperature to 607 °C cycle after the first heating round, which allowed us to compare the initial and post-heating rock magnetic behaviors of measured specimens.

3. Results

3.1. Magnetic carriers within Galapagos lava samples

We calculated M_s, M_{rs}, B_c, and B_{cr} values for each specimen from the rock magnetic curves collected at each low temperature (Fig. 2 and Figs. S1–S4) during LT-TFT experiments. We noted sharp transitions in the M_{rs} vs. temperature curves, as well as in the B_{cr} and B_c vs. temperature curves around 110 K–120 K for specimens GA 79.4v and GA 84.1v (Fig. 2g, h, i, j). In contrast, GA 78.5v, GA 78.2v, GA 79.1v, GA 85.7v, and GA 85.1v exhibited smoother changes in B_c and B_{cr} with temperature, and their M_{rs} curves have a distinct pattern from those of GA 84.1v (Fig. 2a, b, c, d, e, f, k, l, m, n). Differences in the Verwey transition in magnetite with different domain states likely cause these different low-temperature behaviors. The FC-ZFC curves of the GA-Xu specimens also exhibit a more discrete transition around 120 K (Fig. 3), associated with the Verwey transition of magnetite. The FC curves are elevated relative to the ZFC curves, which may indicate the presence of fine magnetite grains (Fig. 3).

From the back-scattered electron (BSE) imaging of the critical specimen GA 84.6u shown in Fig. 4, microscale titanomagnetite grains are contained within the specimen, which commonly exhibits ilmenite lamellae features with I-III deuteric oxidation stage (Wilson and Watkins, 1967) (Fig. 4). Primary titanomagnetite grains with abundant ilmenite lamellae are divided into smaller and brighter iron-rich regions (Fig. 4a-b), which may produce the relative pure magnetite grains with Verwey transition near 120 K in low-temperature measurements. The other titanomagnetite particles within specimen GA 84.6u exhibit near-

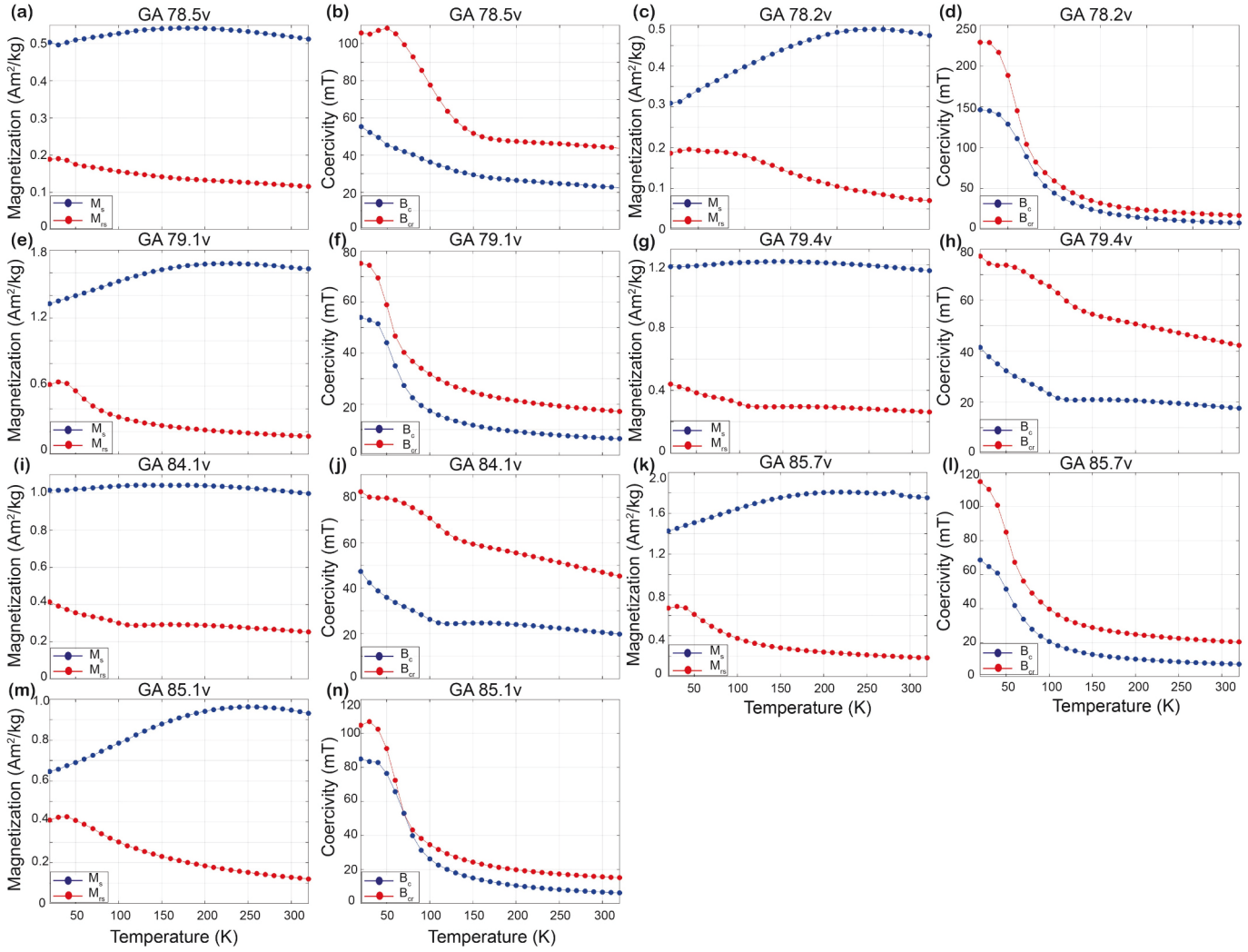

Fig. 2. Low-temperature TFT experiments on fresh ~20 mg chips ("v" specimens) from GA 78.5, GA 78.2, GA 79.1, GA 79.4, GA 84.1, GA 85.7, and GA 85.1. Hysteresis loops and DCD curves were measured at cryogenic temperatures from 20 K to 320 K in 10 K intervals. We calculated hysteresis parameters for each specimen at each temperature, with M_s and M_{rs} shown in the first and the third columns and B_c and B_{cr} shown in the second and fourth columns.

homogeneous features (a few ilmenite lamellae) (Fig. 4c–d). Based on the above results, we indicate that the primary magnetic minerals in Galapagos lava samples are titanomagnetite or low-titanium titanomagnetite, which is consistent with the J_s-T curves obtained from their counterpart "s" specimens in previous studies (Wang and Kent, 2013).

3.2. *Thermal instability of Galapagos lava samples*

3.2.1. *Rock magnetic results after multiple heating-cooling cycles*

We obtained an additional set of rock magnetic curves (Figs. S5 and S6) after the heating treatments and compared the initial and post-heating hysteresis properties (Figs. 5–6 and S7–S8) to assess the thermal stability of the GA-Xi specimens. The GA 84 series specimens (GA 84.1i, GA 84.3i, GA 84.6i), which initially exhibited more SD behavior, display a decrease in hysteresis parameters (M_{rs}, B_c, and B_{cr}) after the first heating to 400 °C (Fig. 5b–d). After undergoing three heating-cooling cycles at 400 °C, these hysteresis parameters remained relatively constant (Fig. 5b–d). Following the first heating to 500 °C, the room-temperature M_{rs} and B_c values increased strongly and followed an increasing trend across the three subsequent heating-cooling cycles to 500 °C (Fig. 5b-c). M_{rs} and B_c in GA 84 series specimens were particularly sensitive to the higher-temperature heating treatment (Fig. 5b-c), suggesting that the thermal alteration was related to changes in the domain configuration. When the heating temperature reaches 500 °C, changes in M_s also show evidence of thermochemical alteration within GA 84 series specimens (Fig. 5a).

Hysteresis parameter ratios of the GA 84 series specimens were calculated, and the results were plotted on a Day diagram (Fig. 5e). These ratios shifted slightly toward the MD region after the first heating to 400 °C and remained constant after three cycles to this temperature. The first heating to 500 °C resulted in significant shifts in the hysteresis ratios of the GA 84 series specimens toward the upper left part of the Day plot (Fig. 5e), indicating a domain state transition from more MD to more SD behavior in these specimens. Therefore, we determined that a higher heating temperature has a much stronger effect on the hysteresis parameters of GA 84, with severe thermal alteration occurring after the first heating to 500 °C.

The GA 78 series specimens (GA 78.2i and GA 78.8i) exhibited hysteresis behavior similar to that of the GA 84 series. Hysteresis parameters relatively change after the first and third heating-cooling cycles to 400 °C (Fig. 5a–d). After the 500 °C heating, M_s and M_{rs} in GA 78.2i increased significantly (Fig. 5a–b), while the magnetization of GA 78.8i decreased sharply (Fig. 5a–b). After three 500 °C heating-cooling cycles, the GA 78 series hysteresis parameters (M_s, M_{rs}, B_c) continued to increase (Fig. 5a–c). The initial domain state of GA 78.2 had less SD-like behavior (Fig. 5e), which exhibited greater thermal changes after the

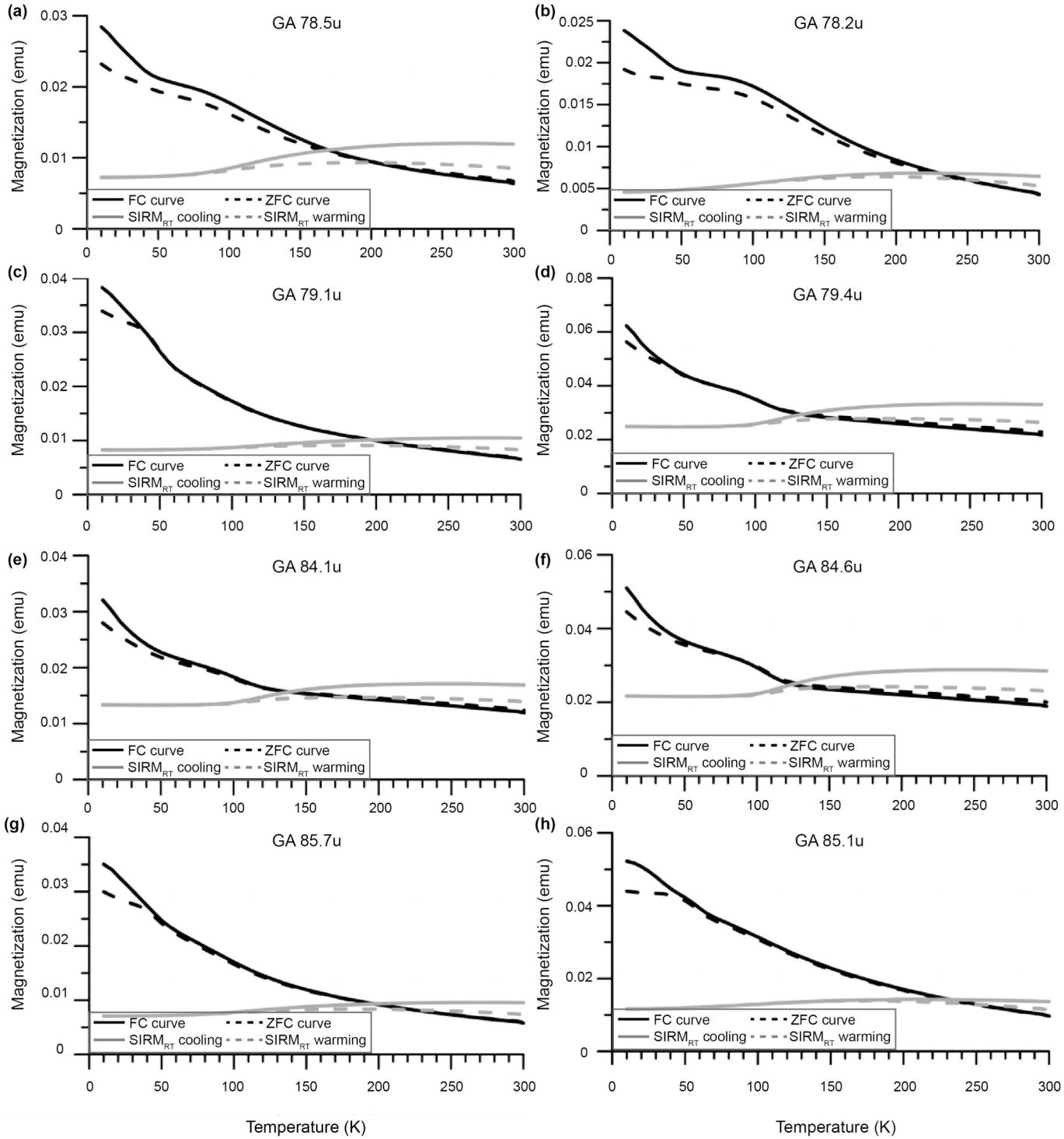

Fig. 3. Low-temperature magnetic property curves (FC-ZFC, SIRM$_{RT}$ cooling, and warming) for Galapagos lava specimens (a) GA 78.5u, (b) GA 78.2u, (c) GA 79.1u, (d) GA 79.4u, (e) GA 84.1u, (f) GA 84.6u, (g) GA 85.7u, and (h) GA 85.1u (Magnetization in arbitrary units). Field-cooled and zero-field cooled (FC ZFC) remanence warming curves (Moskowitz et al., 1993), as well as low-temperature demagnetization (LTD) cooling and warming curves of room temperature saturation isothermal remanence (SIRM$_{RT}$), were measured every 5 K from 10 K to 300 K using a Quantum Designs magnetic properties measuring system (MPMS) in the Institute for Rock Magnetism, University of Minnesota.

first heating to 500 C (Fig. 5). In addition, the changes in hysteresis parameters for the GA 78 series are mainly characterized by shifts in M_s and M_{rs} (Fig. 5a b), indicating that thermal alteration occurred due to thermophysicochemical changes from high-temperature heating treatments.

Differences in the initial hysteresis behavior were observed among the GA 79 series specimens (GA 79.4i, GA 79.5i, GA 79.8i) (Fig. 6). Specifically, GA 79.4i, which displayed more SD behavior, experienced significant changes in M_s, M_{rs}, B_c, and B_{cr} after each heating-cooling cycle, indicating that thermal physical and chemical alteration occurred in this specimen (Fig. 6a d). The hysteresis parameter ratios for GA 79.4i moved toward the SD region in the Day diagram after the

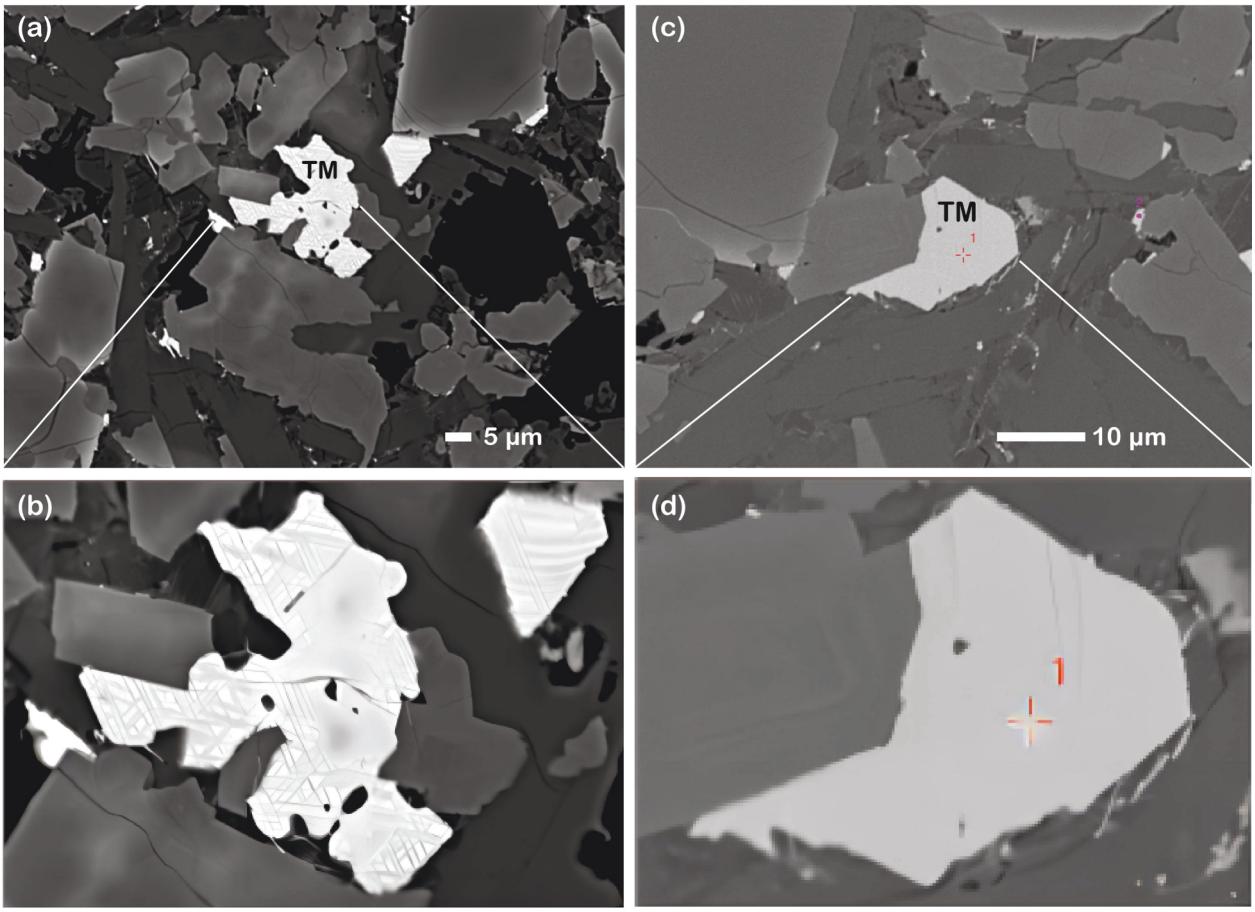

Fig. 4. Back-scattered electron (BSE) images were taken in selected GA-X specimen GA 84.6u. (a, c) Microscale titanomagnetite (TM) grains within the specimen. (b) Titanomagnetite with abundant ilmenite lamellae is observed. Darker ilmenite divides primary titanomagnetite into brighter iron-rich regions with dimensions of less than 10 μm or 1 μm due to deuteric oxidation. (d) Titanomagnetite grain with near homogeneous features (a few ilmenite lamellae features) contained in the specimen. Based on the definition of the stages in high-temperature oxidation within titanomagnetite from Wilson and Watkins (1967), the dominant phases within specimen GA 84.6u were recognized as classes I-III.

initial heating to 500 °C (Fig. 6e). Conversely, GA 79.5i and GA 79.8i exhibited minor variations in hysteresis properties compared to GA 79.4i throughout the heating treatments. There was a slight change in M_{rs} after first heating to 400 °C (Fig. 6b). An increase in M_s, M_{rs}, B_c, and B_{cr} after heating to 500 °C indicated severe thermal changes (Fig. 6a–d).

In GA 85.3i, which exhibited more MD behavior prior to heating, M_s remained relatively constant across each measurement step (Fig. 6a). The other properties (M_{rs}, B_c, and B_{cr}) of the specimen GA 85.3i were reduced and enhanced after the initial heatings to 400 °C and 500 °C, respectively (Fig. 6b–d). In contrast, GA 85.2i showed a marked increase in M_s and M_{rs} accompanied by a decrease in B_c and B_{cr} after the initial heating to 400 °C (Fig. 6a-d). After undergoing three heating-cooling cycles at 400 °C, M_s and M_{rs} decreased. However, when heated to 500 °C, both M_s and M_{rs} increased significantly (Fig. 6a–b), suggesting that GA 85.2i underwent significant thermochemical alteration during the high-temperature heating-cooling cycles.

FORC measurements were performed after each heating treatment for GA-Xi specimens. For the GA 84 series, which initially had more SD behavior, the FORC diagrams of fresh specimens displayed a broad spread along B_u and retained typical contour shapes after single and repeated heatings to 400 °C (Fig. 7a–c). However, significant transformations in the FORC diagrams occurred after the first heating to 500 °C, marked by a significant shift in the central ridge and an increase in the peak of the microcoercivity distribution (Fig. 7a–c). These changes indicate a transition in the magnetic domain state toward more SD behavior. These thermal changes were more pronounced after three heating-cooling cycles to 500 °C (Fig. 7a–c). Therefore, the GA 84 series specimens experience substantial thermal alteration following the initial heating to 500 °C, as evidenced by the changes in hysteresis parameters (Fig. 5). Other specimens exhibiting more SD behavior, such as GA 78.8i and GA 79.4i, also displayed shifts in the central ridge of the FORC diagrams after the first heating to 500 °C, which presents changes in domain states (Fig. 7d-e), similar to the GA 84 series.

In contrast, the GA-Xi specimens with mainly MD behavior (GA 78.2i, GA 79.5i, GA 79.8i, GA 85.2i, and GA 85.3i) had FORC diagrams that retained diverging contour patterns without visible evidence of thermal alteration after heating to different target temperatures (Fig. 8). Based on the changes in hysteresis parameters and the thermal behavior of each specimen, as determined from the rock magnetic properties (Figs. 5 and 6), it appears that the FORC diagrams have limited ability to detect thermal alteration that does not involve domain state changes, such as the thermochemical changes that occurred after heating to 400 °C in GA 85.2i (Fig. 6).

Among the ten selected GA-Xi specimens, the IRM acquisition curves of five specimens (more SD behavior: GA 79.4i, GA 84.1i, and GA 84.3i; mainly MD behavior: GA 79.5i and GA 79.8i) before and after heatings were decomposed into two coercivity components (a high-coercivity component (HC) and a low-coercivity component (LC)) using the MAX UnMix web application (Maxbauer et al., 2016). Fig. S9 shows the coercivity spectrum and component analysis for GA 79.5i and GA 84.3i after each heating treatment. The remaining five specimens could not be successfully unmixed into multiple constituent components, possibly

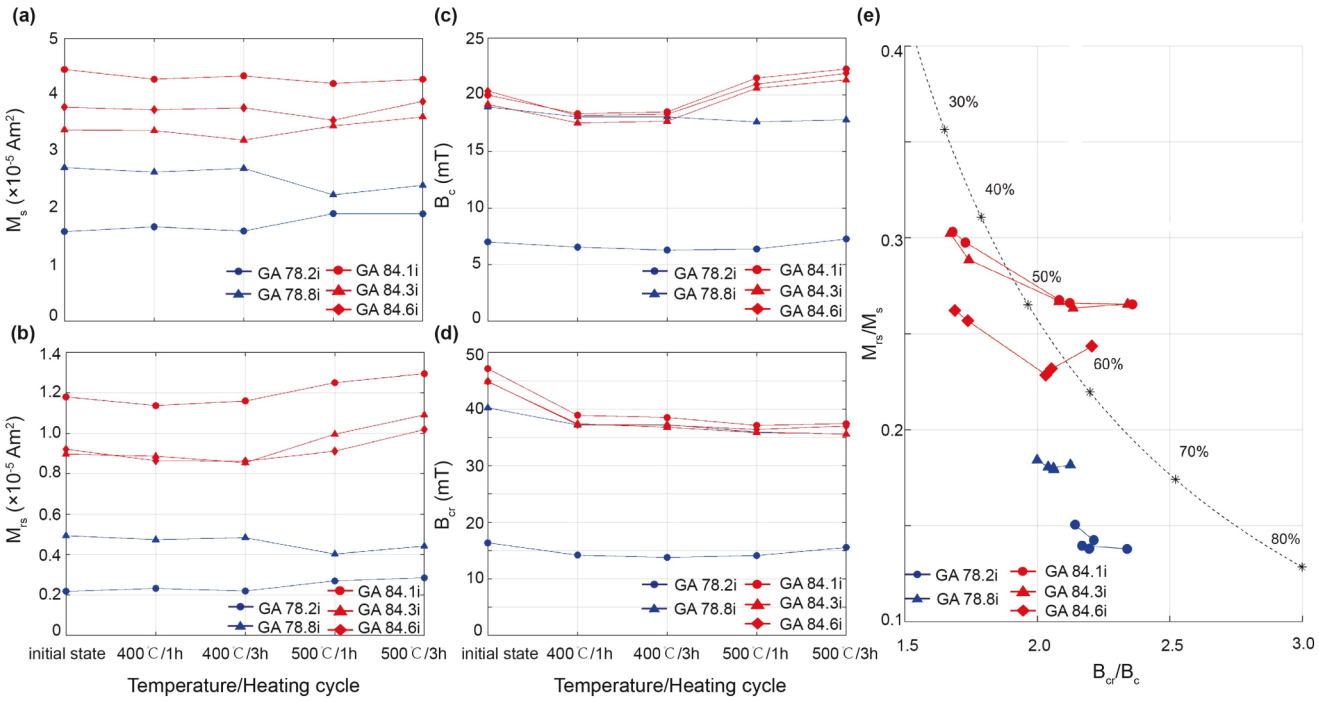

Fig. 5. Hysteresis parameters for GA 78 (blue points) and GA 84 (red points) series specimens were measured at room temperature after each high-temperature heating-cooling treatment. (a) M_s, (b) M_{rs}, (c) B_c, and (d) B_{cr}. (e) Hysteresis parameter ratios are shown in a Day plot. Percentages along the dashed curve are modeled volumes of MD contributions to SSD-MD mixing curve #3 (Dunlop, 2002). (For interpretation of the references to colour in this figure legend, the reader is referred to the web version of this article.)

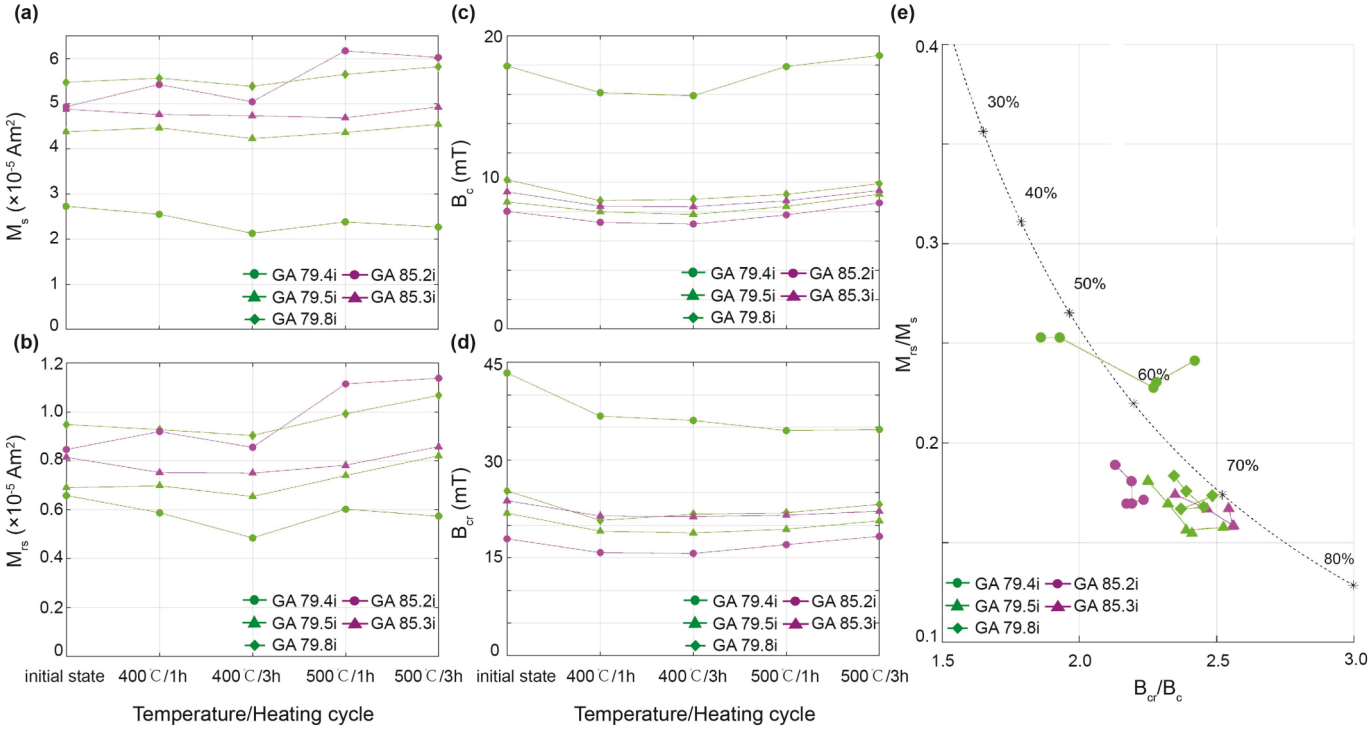

Fig. 6. Hysteresis parameters for GA 79 (green points) and GA 85 (purple points) series specimens were measured at room temperature after each high-temperature heating-cooling treatment. (a) M_s, (b) M_{rs}, (c) B_c, and (d) B_{cr}. (e) Hysteresis parameter ratios are shown in a Day plot. Percentages along the dashed curve are modeled volumes of MD contributions to SSD-MD mixing curve #3 (Dunlop, 2002). (For interpretation of the references to colour in this figure legend, the reader is referred to the web version of this article.)

due to overlapping coercivity spectra of the magnetic carriers they contain.

We also extracted critical parameters, such as $B_{1/2}$ (the applied field at which half of the saturation IRM is acquired), and analyzed the contribution of the remanence of each constituent component from the coercivity spectra (Fig. 9). For more SD specimens (GA 79.4i, GA 84.1i,

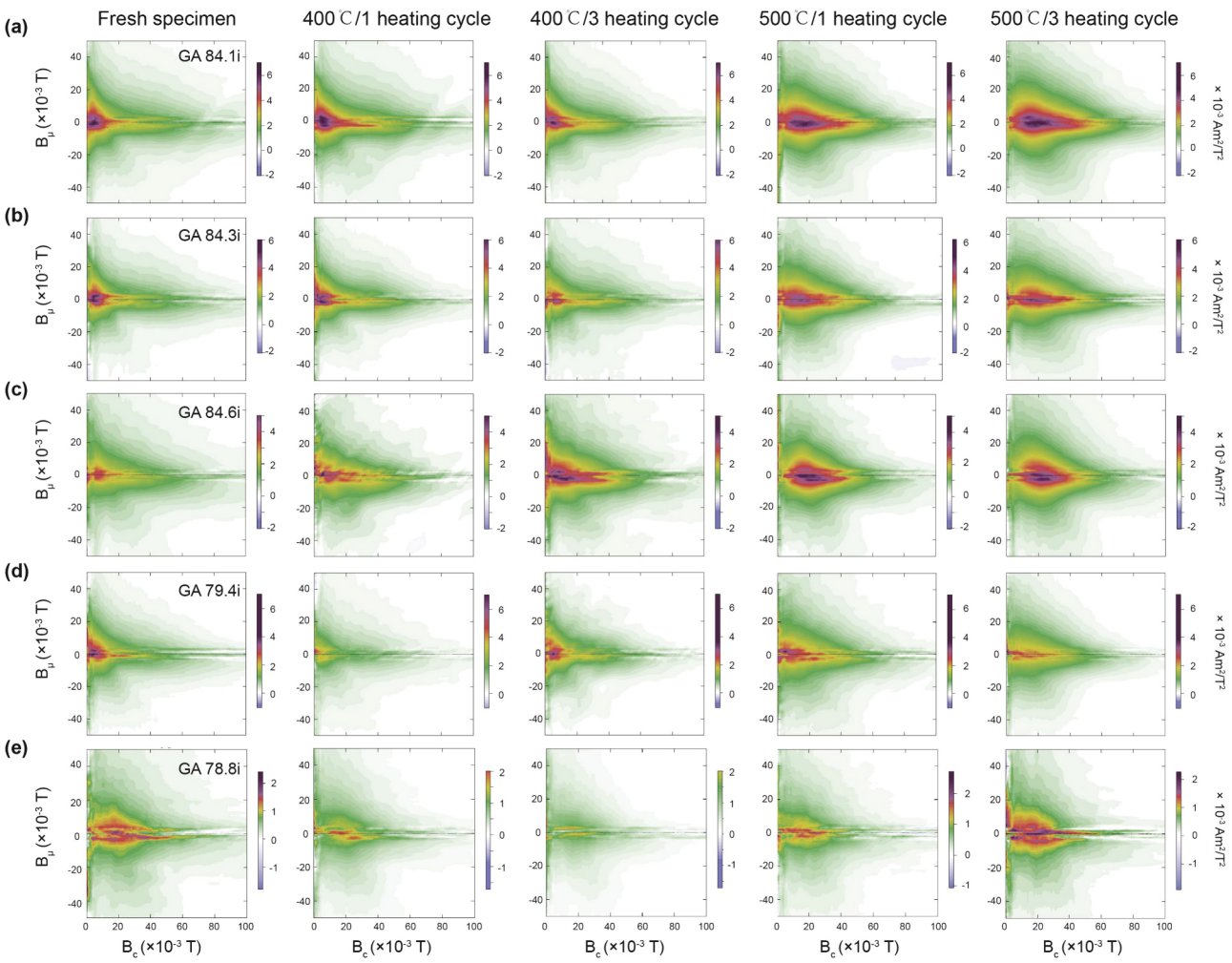

Fig. 7. FORC diagrams for Galapagos lava specimens with more SD behavior (GA 84.1i, GA 84.3i, GA 84.6i, GA 79.4i, and GA 78.8i) after each high-temperature heating-cooling treatment. The FORCinel v3.06 software package (Harrison and Feinberg, 2008) was used to calculate the FORCs (113 FORCs) with a smoothing factor (SF) of 4.

and GA 84.3i), the $B_{1/2}$ of the HC significantly decreased after the first heatings to 400 °C and 500 °C (Fig. 9a), while the contribution of HC to the SIRM exceeded 50% after three 500 °C heating-cooling cycles (Fig. 9b). These variations in the above properties suggest that the hysteresis behavior of the more SD specimens was predominantly influenced by the HC component after high-temperature heating steps. $B_{1/2}$ of the HC in more MD specimens (GA 79.5i and GA 79.8i) exhibited weak changes after heating treatments (Fig. 9c), while the LC demonstrated higher thermal stability through constant $B_{1/2}$ values of the LC before and after each heating step (Fig. 9c). The contribution of the HC to the bulk specimen remanence remained around 75% (Fig. 9d), indicating that the HC dominated the hysteresis behavior in the bulk specimens.

3.2.2. *High-temperature thermal fluctuation tomography experiments*

To gain insight into the thermal stability of measured specimens after heating to near-Curie temperatures, we conducted HT-TFT experiments (Jackson et al., 2006), which allowed us to calculate several critical parameters from the rock magnetic curves (Figs. S10–S13). Fig. 10 shows the M_s, M_{rs}, B_c, and B_{cr} values for each specimen at elevated temperatures. In the repeated measurements (red curves), the M_s curves of GA 84.1w and GA 85.1w remained relatively consistent among the original and repeated experiments (Fig. 10e, g). A significant increase in the M_{rs}, B_c, and B_{cr} curves for these specimens (Fig. 10e–h) indicates that thermal alteration in GA 84.1w and GA 85.1w is more thermophysical than thermochemical. This interpretation is based on the domain-state dependence of M_{rs}, B_c, and B_{cr} in magnetic particles with a given M_s. These observations in GA 84.1w are consistent with our conclusion that the domain state transitioned to more SD behavior and that the remanence carrying capacity increased in this specimen after high-temperature heating treatments (Figs. 5 and 7). After initial heating to near Curie temperature (607 °C), the M_s curves of other specimens (GA 78.5w and GA 79.1w) decreased, with elevated M_{rs} curves in repeated experiments (Fig. 10a, c). This indicates that thermochemical changes occurred during high-temperature heating, enhancing the remanence carrying capacities of these specimens.

In summary, the selected Galapagos lava specimens exhibit thermal instability after heating to 400 °C, obtained from multiple heating-cooling cycle measurements (Figs. 5–7 and S14). From multi-cycles and HT-TFT results, we obtained severe thermal changes that occurred when the heating temperature reached 500 °C, mainly leading to enhanced remanence carrying capacities (Figs. 5–7, 10, and S14). The GA 78 series specimens underwent substantial thermochemical changes after the initial heating to 500 °C (Fig. 5). Specimens GA 79.4 and GA 85.2 experienced thermo-chemical alteration at a target temperature of 400 °C (Fig. 6). Severe thermophysicochemical changes in specimens GA 84 series were mainly characterized by a reduction in effective ferromagnetic grain size after heating above 500 °C (Figs. 5, 7, 10). Hysteresis properties of specimens GA 79.5, GA 79.8, and GA 85.3 decreased relatively below 500 °C and increased in M_{rs}, B_c, and B_{cr} upon heating to

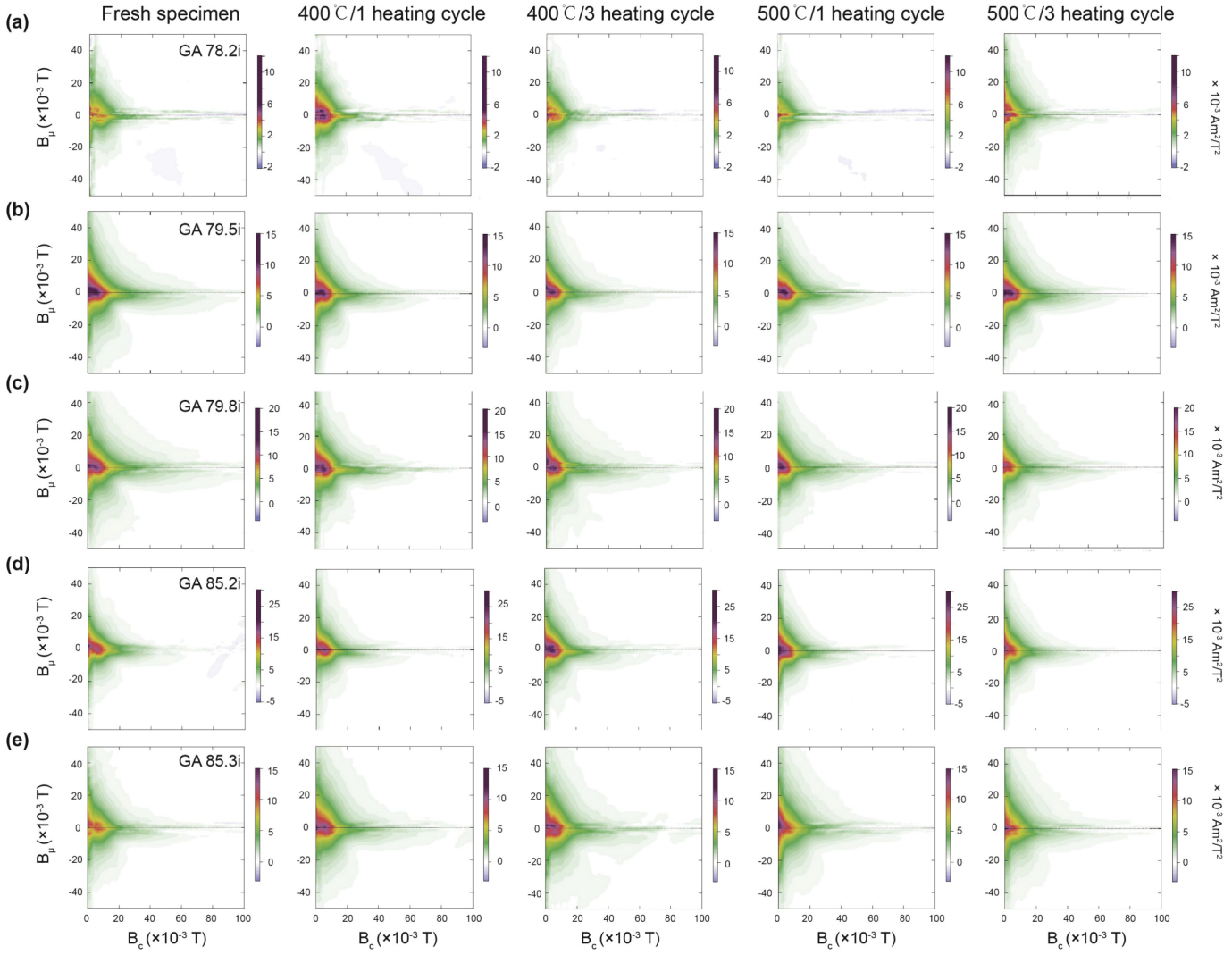

Fig. 8. FORC diagrams for Galapagos GA-X specimens with mainly MD behavior (GA 78.2i, GA 79.5i, GA 79.8i, GA 85.2i, and GA 85.3i) after high-temperature heating treatments. The FORCinel v3.06 software package (Harrison and Feinberg, 2008) was used to calculate the FORCs (113 FORCs) with a smoothing factor (SF) of 4.

500 °C (Figs. 6, 10).

4. Discussion

4.1. Underestimation of paleointensity records during SRE event

Based on the comprehensive rock magnetic measurements described above, the thermal changes of GA-X samples that occurred after the heating steps at critical temperatures (400 °C, 500 °C, and 607 °C) may result in biased paleointensity estimates calculated from the above critical temperature intervals (400 °C–575 °C). Therefore, we attempt to utilize the thermal instability of these samples to analyze and discuss the reliability of their paleointensities from previous RESET methods (Wang and Kent, 2013, 2021). In order to correct the non-linear Arai plot caused by the lack of reciprocity of MD grains, the RESET method subjects measured specimens to a total thermoremanent magnetization (tTRM) from the Curie temperature in a known laboratory field after the original Thellier-Coe experiment. Then, the same paleointensity procedure is repeated, and a corrected Arai diagram is obtained by plotting the natural remanent magnetization (NRM) remaining (unblocking) against the tTRM unblocking (Wang and Kent, 2013, 2021).

In order to interpret and understand the paleointensity results of Galapagos lavas, we display hysteresis parameter M_{rs} after critical temperature heating steps combined with original Arai plots with similar two-slope behavior of GA 84 and GA 79 series specimens, which are shown in Fig. 11. For the GA 84 series specimens with more SD behavior, there was a slight decrease in M_{rs} after the first 400 °C heating and a sharp increase in M_{rs} after heating above 500 °C (Fig. 11a). The two-slope behavior Arai plots of GA 84 series specimens are mainly attributed to thermal changes in the specimens during the paleointensity experiment (Fig. 11b and Fig. S15a–b). For heating temperatures below 500 °C, changes in magnetic domain state lead to decreased remanence-carrying capacity for remanent magnetization, which reduces the acquisition of partial thermoremanent magnetization, resulting in overestimated paleointensity values in this temperature interval (Fig. 11b and Fig. S15a–b). As the heating temperature reaches 500 °C, a significant enhancement in M_{rs} increases microcoercivity and TRM carrying efficiency, leading to shallower NRM-pTRM slopes in the higher-temperature range (500 °C–575 °C) (Fig. 11a–b). A similar situation occurred in the GA 79 series specimens, but they displayed more thermal stability than the GA 84 series (Fig. 11c–d and Fig. S15c–d).

For the GA 78.2i specimen, thermochemical changes occurred following heating treatments first at 400 °C and 500 °C (Fig. 12a), which enhanced the remanence carrying capacities and resulted in the biased to low value from the high-temperature segment (400 °C–575 °C) in the original Arai plot of specimen GA 78.2c (Fig. 12b). Conversely, the

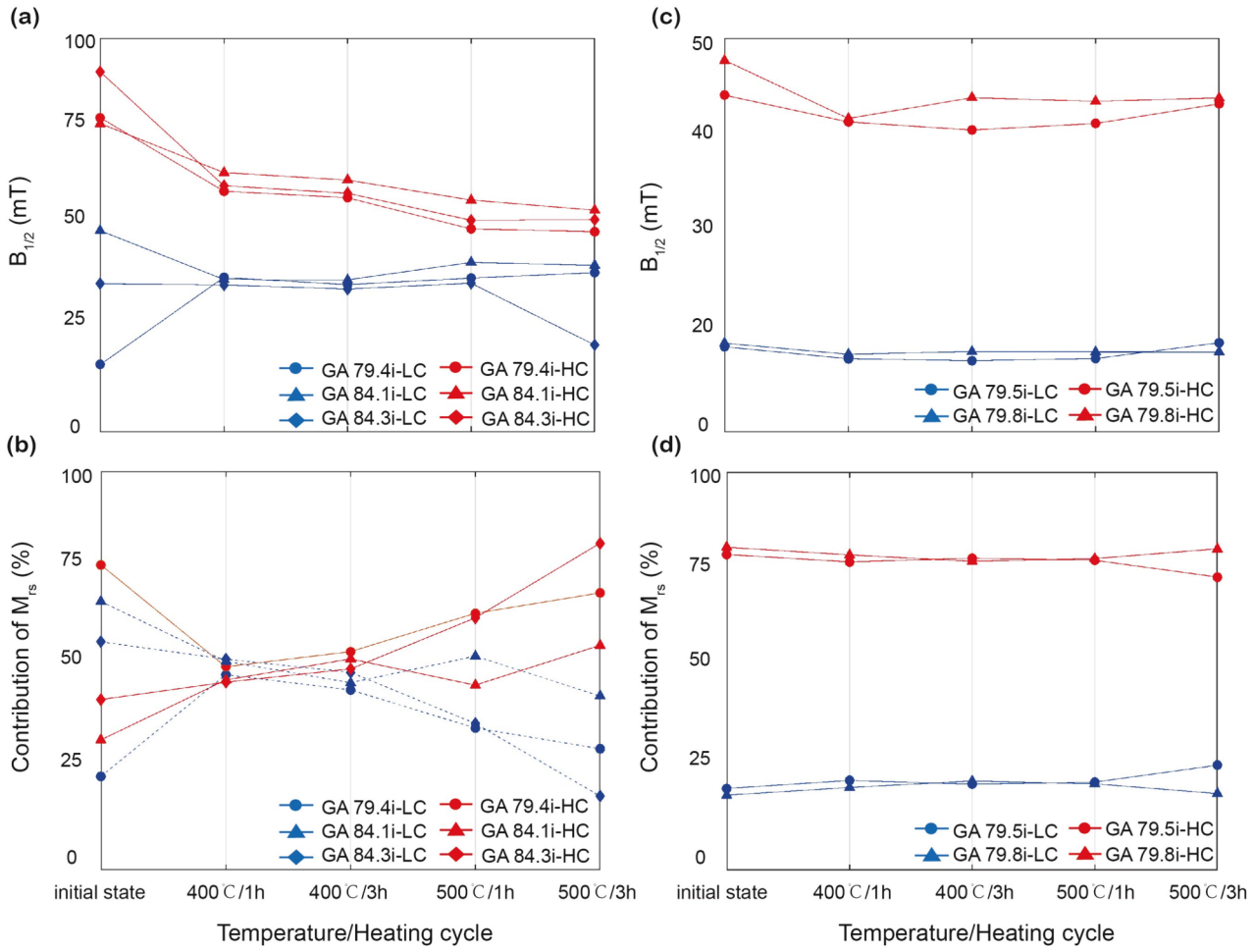

Fig. 9. (a, b) Hysteresis parameters ($B_{1/2}$ and contribution to SIRM) for the LC and HC of specimens with more SD behavior (GA 79.4i, GA 84.1i, and GA 84.3i) after each heating treatment. (c, d) Hysteresis parameters ($B_{1/2}$ and contribution to SIRM) for the LC and HC of specimens with more MD behavior (GA 79.5i and GA 79.8i). The above magnetic parameters were calculated from unmixed IRM acquisition curves using the MAX UnMix web application (Maxbauer et al., 2016).

reduced values of M_{rs} after 400 °C and 500 °C heating steps lead to decreased carrying capacities for remanence of GA 78.8i, which overestimated paleointensity value fitting by 400 °C–575 °C intervals (Fig. 12c). Specimen GA 85.2i showed increases in M_s and M_{rs} after initial heatings to 400 °C and 500 °C, enhancing its ability to acquire pTRM in paleointensity experiments (Fig. 12d). These changes decreased the slope of the Arai diagram and potentially caused the paleointensity from the 400 °C–575 °C interval to be underestimated (Fig. 12e). Moreover, the decrease in M_{rs} after initial heating to 400 °C and increased at 500 °C for specimen GA 85.3i, leading to a two-slope Arai plot and underestimating paleointensity value from the high-temperature segment (Fig. 12f).

In summary, the in-depth experiments on rock magnetism and analysis of hysteresis parameters for Galapagos lava samples determined that the thermal instability primarily accounts for the behavior of Arai diagrams of GA-Xc specimens and biased paleointensities (Figs. 11, 12, S14). For two-slope Arai diagrams, heating steps below 500 °C decrease the remanent magnetization-carrying capacity of the samples. In contrast, heating treatment above 500 °C markedly increases the samples' ability to record remanent magnetization, leading to underestimating paleointensities by fitting high-temperature intervals from original Arai diagrams. The capacity to carry remanence is enhanced for most GA-X lava samples due to heating at temperatures exceeding 500 °C, which promotes the sample's capacity to obtain tTRM in repeated Thellier-Coe experiments and results in an erroneous low estimation of paleointensities from the RESET corrected Arai plots.

Although the Galapagos lava samples are valuable recorders that provide the opportunity for paleointensity studies during a short-lived geomagnetic excursion event (SRE) from a near-equator region, the thermal instability of measured samples biased the strength of the Earth's magnetic field and the extremely low paleointensities obtained from Wang and Kent (2013; 2015) are underestimated. Therefore, in further studies, we will attempt to collect more lava samples from the Galapagos GA-X site and select thermal stability lavas to reveal the mechanism of the geomagnetic field behavior during the SRE through accurate paleointensity determinations.

4.2. The strengths of rock magnetic methods for thermal change detections and paleointensity interpretations

In our detailed rock magnetic experiments, we obtain critical hysteresis properties at ambient and elevated temperatures to detect the thermal alteration within the measured specimens and reveal the sources of these changes (Figs. 5, 6, 9, 10). These hysteresis parameters (e.g., M_s, M_{rs}, and B_c) are crucial indicators of thermochemical alteration, fluctuations in the remanence carrying capacity, and changes in domain states in measured samples. We detect the thermal instability in each GA-X specimen when heated to 400 °C, due to changes in hysteresis parameters after multiple heating-cooling cycles (Figs. 5, 6, S14). For instance, the reduction in hysteresis parameters (M_{rs}, B_c, and B_{cr}) in GA 84 series specimens following initial heating to 400 °C demonstrates the thermophysical alteration in these specimens (Fig. 5). The severe

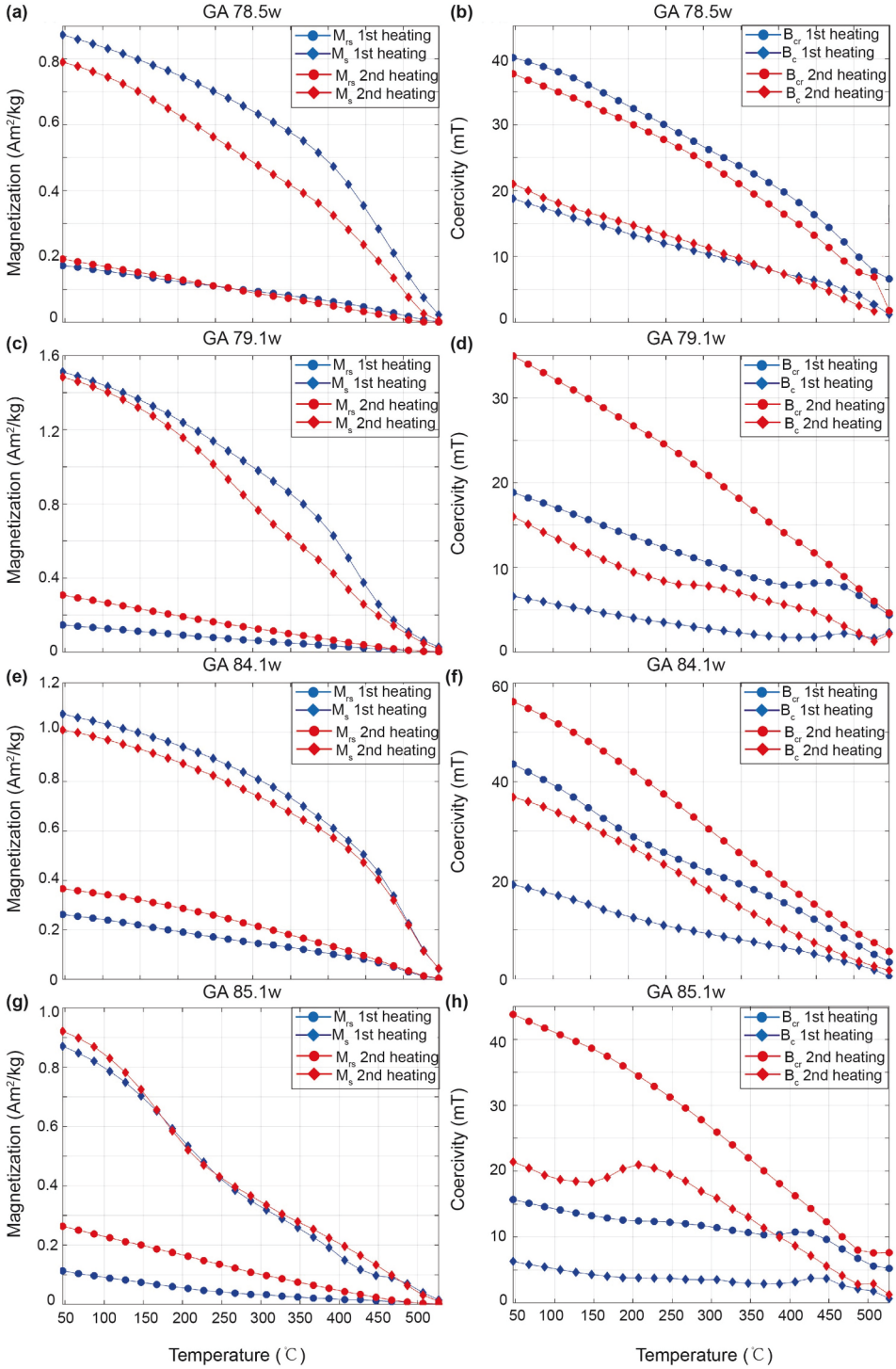

Fig. 10. Temperature-dependent hysteresis measurements from room temperature to ~600 °C. (a, c, e, g) M_{rs} and M_s curves; (b, d, f, h) B_{cr} and B_c curves for Galapagos lava specimens GA 78.5w, GA 79.1w, GA 84.1w, and GA 85.1w. Blue curves represent the first heating treatment; red curves represent the repeated heating treatment. (For interpretation of the references to colour in this figure legend, the reader is referred to the web version of this article.)

thermal changes occurred when the heating temperature reached 500 °C, primarily evident in elevated M_{rs} values of GA-X specimens, indicating increased remanence-carrying capacities (Figs. 5, 6, S14), such as the increased M_s and M_{rs} values of specimen GA 78.2i (Fig. 5). The HT-TFT experiments revealed that thermal alteration occurred after 607 °C heating steps, primarily enhancing the carrying capacities for remanent magnetizations (Fig. 10 and Fig. S14). For example, after initial heating to near Curie temperature, the thermophysical alteration was observed in specimen GA 84.1w obtained from enhanced M_{rs}, B_c, and B_{cr} values (Fig. 10). Therefore, the critical hysteresis properties, as the powerful thermal change indicators, recognized the thermal instability of Galapagos lava samples after heating treatments higher than 400 °C and revealed the sources of these thermal changes (Figs. 5, 6, 10, S14).

A strength of our rock magnetic methods for paleointensity evaluations is attributed to the focus on hysteresis parameters variations after heating steps at critical temperatures (400 °C, 500 °C, 607 °C), which were derived from the temperature segments (400 °C–575 °C) to

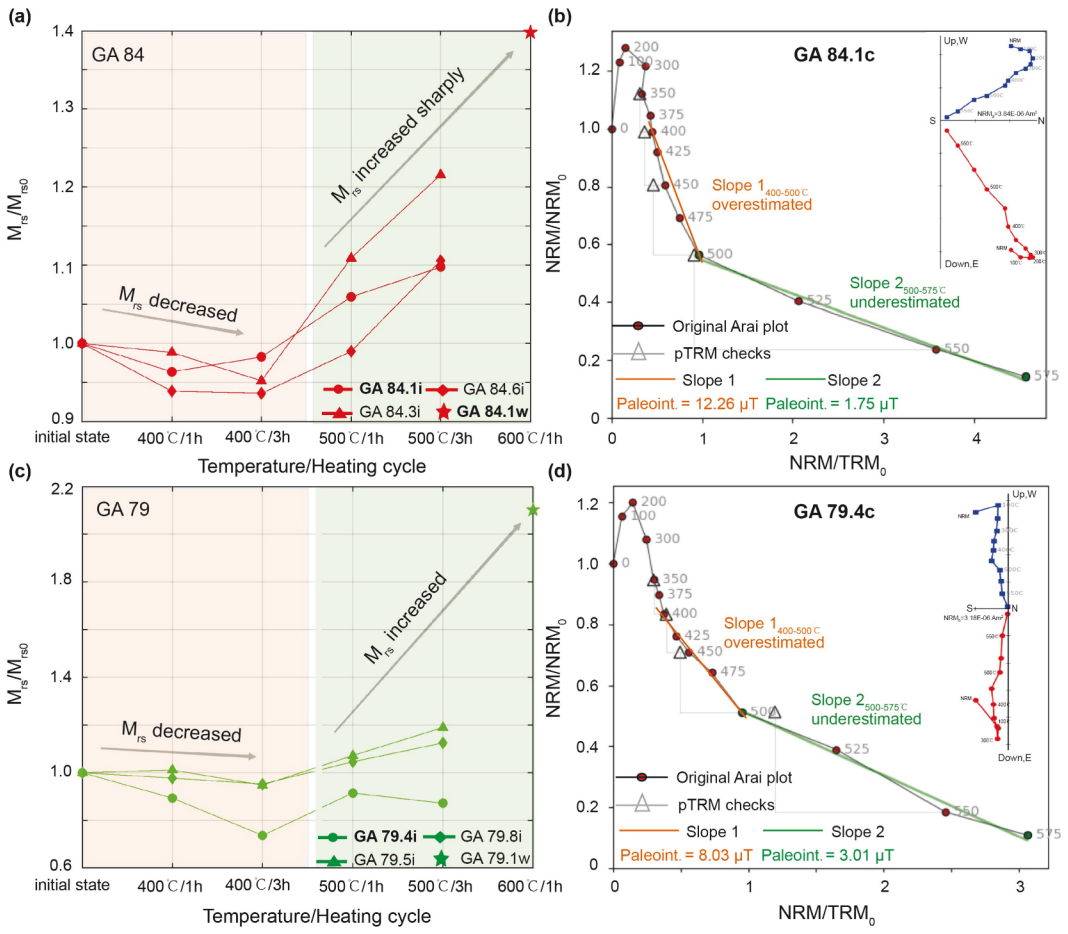

Fig. 11. Hysteresis parameters analysis for paleointensity interpretations with two-slope Arai plots. (a, c) Critical hysteresis parameter M_{rs} for GA 84 (red points) and GA 79 (green points) series specimens were measured at room temperature after each critical multi-heating-cooling treatment (400 °C, 500 °C) on "i" specimens. The HT-TFT experiments for "w" specimens provide the value of M_{rs} after ~600 °C heating treatments. M_s, B_c, and B_{cr} vs. critical temperature curves are exhibited in Fig. S7. Hysteresis parameters are normalized to the initial room temperature value before the heating steps (such as M_{rs0}). (b, d) Two-slope Arai plots for specimens GA 84.1c and GA 79.4c, with figures and captions modified from Wang and Kent, 2013. Similar behavior Arai plots for the other four specimens, GA 84.3c, GA 84.6c, GA 79.5c, and GA 79.8c, are shown in Fig. S15. In Arai diagrams, the orange line indicates paleointensity estimates obtained by fitting the segment of 400 °C–500 °C, and the green line indicates paleointensity obtained by fitting the higher-temperature data (500 °C–575 °C). Grey triangles represent pTRM checks. The inset in each Arai diagram shows the NRM thermal demagnetization vector diagrams for "b" specimens (modified from Wang and Kent (2013)). Blue points indicate vector end-points projected onto the horizontal plane, red points indicate vector end-points projected onto the vertical plane, and numbers adjacent to data points are demagnetization temperatures. (For interpretation of the references to colour in this figure legend, the reader is referred to the web version of this article.)

determine the GA-X samples' paleointensities in previous studies. By scrutinizing the hysteresis parameters above, the thermal instability of samples after heating steps from 400 °C was precisely determined, leading us to confirm that thermal changes have biased the current paleointensities fitting by higher temperature segments, including from 400 °C to ~600 °C (Figs. 11 and 12). Furthermore, the susceptibilities measurements for Galapagos paleointensity specimens (GA-Xc) also demonstrated the thermal instability exhibited by 400 °C heating treatment, which displayed a reduced trend from 400 °C and a 20–40% decrease in susceptibility after first heating to 575 °C in the original paleointensity experiment (Fig. S16) (Wang and Kent, 2013). Compared to detailed rock magnetic experiments, susceptibilities measurements can be easier to indicate magnetic carriers' alteration of GA-Xc specimens at which temperature, but understanding the process and source of thermal alteration needs to be combined with critical hysteresis properties analysis from detailed rock magnetic experiments (Figs. 11, 12, S14).

The rock magnetic methods also provide another efficient detection method to recognize the thermal instability of samples during paleointensity experiments, which may have been hidden in conventional check methods, such as the thermal changes of GA 84.6c hidden in passed pTRM checks (Fig. 11a and Fig. S15b). This is a potential risk that the paleointensity estimates might be biased due to the thermal alteration of the above specimens, which results in the current underestimation of paleointensities from GA-X lavas during the SRE interval. Therefore, rock magnetic methods independent of paleointensity experiments for evaluating the thermal stability of samples are extremely important, which help to select suitable paleointensity samples combined with conventional check methods to obtain high-fidelity paleointensity estimates.

Analyzing rock magnetic results to evaluate thermal stability enabled us to interpret paleointensities thoroughly. As an illustration, the GA 84 series specimens' two-slope Arai diagrams primarily originate from various thermal alterations triggered by differing heating temperatures, where experiments below 500 °C lead to a reduced capacity for remanent magnetization, and when heated to 500 °C or above, remanent magnetization carrying capacity enhanced (Fig. 11a-b). Although non-ideal Arai diagrams could stem from multiple causes in practical experiments, such as multidomain (MD) effects (e.g., Riisager and Riisager, 2001; Xu and Dunlop, 2004; Biggin, 2006; Shaar et al., 2011; Wang and Kent, 2013; Smirnov et al., 2017), and thermochemical remanent magnetization (TCRM) production in the laboratory heating

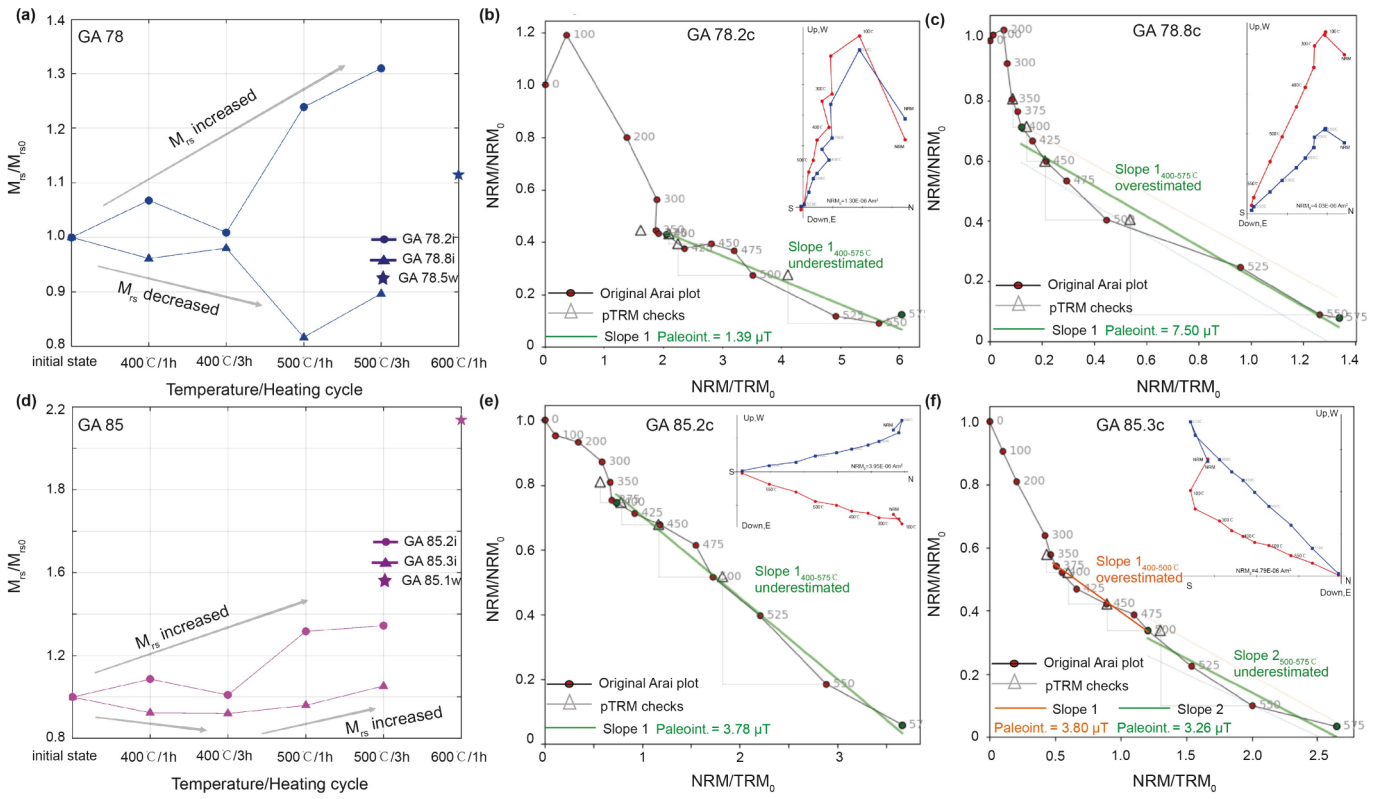

Fig. 12. Hysteresis parameters analysis for paleointensity interpretations. (a, d) Normalized critical hysteresis parameter (normalized to the M_{rs0}) for GA 78 (blue points) and GA 85 (purple points) series specimens were measured at room temperature after heatings at 400 °C, 500 °C, ~600 °C. M_s, B_c, and B_{cr} vs. critical temperature curves are exhibited in Fig. S7. Arai plots for specimens GA 78 (b, c) and GA 85 (e, f), with figures and captions modified from Wang and Kent (2013). In Arai diagrams, the green line indicates paleointensity obtained by fitting the temperature interval from 400 °C to 575 °C. Grey triangles represent pTRM checks. The inset in each Arai diagram shows the NRM thermal demagnetization vector diagrams for "b" specimens (modified from Wang and Kent (2013)). Blue points indicate vector end-points projected onto the horizontal plane, red points indicate vector end-points projected onto the vertical plane, and numbers adjacent to data points are demagnetization temperatures. For specimen GA 85.3i, the hysteresis behavior was similar to GA 79 and GA 84, which exhibited the two-slope Arai plots (the orange line indicates paleointensity estimates obtained by fitting from 400 °C–500 °C, and the green line indicates paleointensity obtained by fitting the higher-temperature data (500 °C–575 °C)). (For interpretation of the references to colour in this figure legend, the reader is referred to the web version of this article.)

steps or initial cooling process (Yamamoto et al., 2003), the thermal changes of samples stand out as a critical element that demands attention. Consequently, an in-depth analysis of rock magnetism for measured samples can aid in detecting the thermal changes of measured samples, which can help us assess the reliability of obtained paleointensity estimates.

In addition, some Galapagos lava samples maintain thermal stability under experimentally appropriate high-temperature heating treatments. For example, the specimen GA 79.5i retains relative thermal stability when the heating steps reach 400 °C (Fig. 6a-b). Therefore, we considered that the appropriate temperature heating steps set would guide the improvement of paleointensity experimental procedures. Future studies should identify the critical temperatures at which the sample remains thermally stable, as obtained from detailed rock magnetic results after successive heating steps. Secondly, adjusting the maximum heating temperature from the Curie temperature to a lower critical target temperature during the paleointensity experiments to prevent thermal changes in samples and highlight the ideal behavior of the TRM spectrum at low temperatures (Coe, 1967a), which improves the success rate of paleointensity experiments. However, the remanent magnetization components with lower blocking temperatures often carry secondary remanent magnetization, especially in ancient rock samples. As a result, detailed analysis of the intrinsic characteristics of the measured samples, such as the age of lava samples, remanent magnetization components contained, magnetic carriers, and thermal stability of samples, are crucial in guiding the improvement of paleointensity experimental procedures.

Finally, our detailed rock magnetic measurements are not without limitations. Heavy complementary rock magnetic experiments, including multiple heating-cooling cycles and HT-TFT experiments, will lead to an additional experimental time of about several hours for each specimen. It is necessary to optimize experimental steps in further studies. Considering the low sensitivity and time-consuming of the FORC measurements for detecting thermal changes, in practical experiments, the hysteresis loops and remanent magnetization curves can provide a sufficient description for assessing the samples' thermal stability, which will reduce the measured time. There is a potential risk in detecting thermal changes within paleointensity specimens through rock magnetic measurements on sister specimens because a lava flow is not perfectly homogeneous (de Groot et al., 2014b). Based on susceptibilities measurements and comprehensive rock magnetic experiments, we observe comparable rock magnetic behaviors between GA-Xc and rock magnetic specimens, such as the susceptibilities and hysteresis properties changes after heating to 400 °C, indicating the relative internal consistency among GA-X specimens. Thus, the rock magnetic behavior of sister specimens from each Galapagos lava sample can demonstrate the hysteresis behavior of the paleointensity specimen (GA-Xc). In summary, a detailed rock magnetic experimental procedure (Fig. S14) should be used to evaluate the fidelity of previous paleointensity records during critical geohistorical intervals, such as the geomagnetic excursion event, which will help us to understand the Earth's magnetic field evolution. For new paleofield studies, it is necessary to preselect lava samples with thermal stability and set appropriate maximum target temperatures to improve paleointensity

procedures and success rate.

5. Conclusions

Through comprehensive rock magnetic experiments and detailed analysis of hysteresis properties after multiple heating treatments at critical temperatures (400 C, 500 C, and 607 C), we confirm the thermal instability of Galapagos lava samples to remove extremely low paleointensities from accurate records during the SRE event. We identified the sources of thermal alteration and noted the thermal instability of GA-X samples after heating to 400 C. When the heating temperature was higher than 500 C, significant thermal changes occurred, which led to increased remanence-carrying capacities and shallower the slope of Arai diagrams. These above critical findings confirm that the extremely low values of paleofield strength during the SRE recorded in Galapagos lava flows are underestimated. Consequently, in-depth analysis of rock magnetic results can evaluate the fidelity of current paleointensity estimates, and future paleomagnetism research can benefit from rock magnetic experiments for sample preselecting to refine experimental procedures for paleofield strength determinations. Additionally, we will select thermal stability lava samples from worldwide to obtain paleofield strength records during SRE and reveal the ability of the Earth s magnetic field to change on millennial scales in future studies.

Author statements

This manuscript is an original work. It has not been published previously and is not being considered for publication elsewhere. All authors approve of the submission.

Our manuscript contains 7,285 words, 12 figures, and a supplementary information file.

CRediT authorship contribution statement

Junxiang Miao: Writing original draft, Writing review & editing, Conceptualization, Visualization, Validation. **Huapei Wang**: Writing review & editing, Validation, Methodology, Conceptualization, Resources, Project administration.

Declaration of competing interest

The authors declare that they have no known competing financial interests or personal relationships that could have appeared to influence the work reported in this paper.

Data availability

All the rock magnetic data for Galapagos lava samples measured in this study are available in the Supplemental Information file to all readers.

Acknowledgments

We thank Pierre Rochette for providing Galapagos lava samples via Dennis V. Kent. We are grateful to the Institute for Rock Magnetism (IRM) at the University of Minnesota for supporting Huapei Wang with the visiting fellowship, which allowed low-temperature measurements (LT-TFT and FC-ZFC curve) to be measured. We are also grateful to the Rutgers Paleomagnetic Laboratory for supporting the high-temperature rock magnetic measurements that have been conducted. This research was supported by the Natural Science Foundation of China (41874079).

Appendix A. Supplementary data

Supplementary data to this article can be found online at https://doi.org/10.1016/j.pepi.2024.107225.

References

Balbas, A., Koppers, A.A.P., Kent, D.V., Konrad, K., Clark, P.U., 2016. Identification of the short-lived Santa Rosa geomagnetic excursion in lavas on Floreana Island (Galapagos) by $^{40}Ar/^{39}Ar$ geochronology. Geology 44, 359 362.

Biggin, A., 2006. First-order symmetry of weak-field partial thermoremanence in multi-domain (MD) ferromagnetic grains: 2. Implications for Thellier-type palaeointensity determination. Earth Planet. Sci. Lett. 245, 454 470.

Bono, R.K., Tarduno, J.A., Nimmo, F., Cottrell, R.D., 2019. Young inner core inferred from Ediacaran ultra-low geomagnetic field intensity. Nat. Geosci. 12, 143 147.

Carvallo, C., Roberts, A.P., Leonhardt, R., Laj, C., Kissel, C., Perrin, M., Camps, P., 2006. Increasing the efficiency of paleointensity analyses by selection of samples using first-order reversal curve diagrams. J. Geophys. Res. Solid Earth 111, 15.

Channell, J.E.T., 2017. Magnetic excursions in the late Matuyama Chron (Olduvai to Matuyama-Brunhes boundary) from North Atlantic IODP sites. J. Geophys. Res. Solid Earth 122, 773 789.

Channell, J.E.T., Mazaud, A., Sullivan, P., Turner, S., Raymo, M.E., 2002. Geomagnetic excursions and paleointensities in the Matuyama Chron at Ocean Drilling Program Sites 983 and 984 (Iceland Basin). J. Geophys. Res. Solid Earth 107, 16.

Coe, R.S., 1967a. The determination of paleo-intensities of the Earth s magnetic field with emphasis on mechanisms that could cause non-ideal behavior in Thellier s method. J. Geomagn. Geoelectr. 19, 157 178.

Coe, R.S., 1967b. Paleo-intensities of the Earth s magnetic field determined from tertiary and quaternary rocks. J. Geophys. Res. 72, 3247 3262.

de Groot, L.V., Dekkers, M.J., Visscher, M., ter Maa, G.W., 2014a. Magnetic properties and paleointensities as function of depth in a Hawaiian lava flow. Geochem. Geophys. Geosyst. 15, 1096 1112.

de Groot, L.V., Fabian, K., Bakelaar, I.A., Dekkers, M.J., 2014b. Magnetic force microscopy reveals meta-stable magnetic domain states that prevent reliable absolute palaeointensity experiments. Nat. Commun. 5, 10.

de Groot, L.V., Béguin, A., Kosters, M.E., van Rijsingen, E.M., Struijk, E.L.M., Biggin, A.J., Hurst, E.A., Langereis, C.G., Dekkers, M.J., 2015. High paleointensities for the Canary Islands constrain the Levant geomagnetic high. Earth Planet. Sci. Lett. 419, 154 167.

Doell, R.R., Dalrymple, G.B., 1966. Geomagnetic Polarity Epochs: A New Polarity Event and the Age of the Brunhes-Matuyama Boundary. Science 152, 1060 1061.

Dunlop, D.J., 2002. Theory and application of the Day plot (M_{rs}/M_s versus H_{cr}/H_c) 2. Application to data for rocks, sediments, and soils. J. Geophys. Res. 107, EPM1 EPM15.

Grappone, J.M., Russell, J.M., Biggin, A.J., 2021. Investigating the utility of a high-temperature Thellier-style paleointensity experimental protocol. Earth Planets Space 73, 10.

Harrison, R.J., Feinberg, J.M., 2008. FORCinel: An improved algorithm for calculating first-order reversal curve distributions using locally weighted regression smoothing. Geochem. Geophys. Geosyst. 9, 11.

Hawkins, L.M., Biggin, A.J., Liu, Y.B., Grappone, J.M., Li, Z.X., 2023. Palaeomagnetic field intensity measurements from the 2.6 Ga Yandinilling dyke swarm (Western Australia). Geophys. J. Int. 236, 431 442.

Horng, C.S., Lee, M.Y., Palike, H., Wei, K.Y., Liang, W.T., 2002. Astronomically calibrated ages for geomagnetic reversals within the Matuyama chron. Earth Planets Space 54, 679 690.

Jackson, M., Carter-Stiglitz, B., Egli, R., Solheid, P., 2006. Characterizing the superparamagnetic grain distribution f(V,H_k) by thermal fluctuation tomography. J. Geophys. Res. Solid Earth 111.

Jeong, D., Liu, Q., Yamamoto, Y., Yu, Y., Zhao, X., Qin, H., 2021. New criteria for selecting reliable Thellier-type paleointensity results from the 1960 Kilauea lava flows, Hawaii. Earth Planets Space 73, 10.

Kent, D.V., Wang, H., Rochette, P., 2010. Equatorial paleosecular variation of the geomagnetic field from 0 to 3 Ma lavas from the Galapagos Islands. Phys. Earth Planet. Inter. 183, 404 412.

Kim, W., Doh, S.J., Yu, Y., 2018. Reliable paleointensity determinations from Late Cretaceous volcanic rocks in Korea with constraint of thermochemical alteration. Phys. Earth Planet. Inter. 279, 47 56.

Kosterov, A.A., Pre vot, M., 1998. Possible mechanisms causing failure of Thellier palaeointensity experiments in some basalts. Geophys. J. Int. 134, 554 572.

Maxbauer, D.P., Feinberg, J.M., Fox, D.L., 2016. MAX UnMix: A web application for unmixing magnetic coercivity distributions. Comput. Geosci. 95, 140 145.

Moskowitz, B.M., Frankel, R.B., Bazylinski, D.A., 1993. Rock magnetic criteria for the detection of biogenic magnetite. Earth Planet. Sci. Lett. 120, 283 300.

Qin, H., He, H., Liu, Q., Cai, S., 2011. Palaeointensity just at the onset of the Cretaceous normal superchron. Phys. Earth Planet. Inter. 187, 199 211.

Riisager, P., Riisager, J., 2001. Detecting multidomain magnetic grains in Thellier palaeointensity experiments. Phys. Earth Planet. Inter. 125, 111 117.

Rochette, P., Ben Atig, F., Collombat, H., Vandamme, D., Vlag, P., 1997. Low paleosecular variation at the equator: a paleomagnetic pilgrimage from Galapagos to Esterel with Allan Cox and Hans Zijderveld. Geol. Mijnb. 76, 9 19.

Shaar, R., Ron, H., Tauxe, L., Kessel, R., Agnon, A., 2011. Paleomagnetic field intensity derived from non-SD: Testing the Thellier IZZI technique on MD slag and a new bootstrap procedure. Earth Planet. Sci. Lett. 310, 213 224.

Simon, Q., Bourlès, D.L., Thouveny, N., Horng, C.S., Valet, J.P., Bassinot, F., Choy, S., 2018. Cosmogenic signature of geomagnetic reversals and excursions from the Réunion event to the Matuyama Brunhes transition (0.7 2.14 Ma interval). Earth Planet. Sci. Lett. 482, 510 524.

Singer, B.S., 2014. A Quaternary geomagnetic instability time scale. Quat. Geochronol. 21, 29 52.

Singer, B.S., Hoffman, K.A., Chauvin, A., Coe, R.S., Pringle, M.S., 1999. Dating transitionally magnetized lavas of the late Matuyama Chron: Toward a new $^{40}Ar/^{39}Ar$ timescale of reversals and events. J. Geophys. Res. 104, 679 693.
Smirnov, A.V., Tarduno, J.A., 2003. Magnetic hysteresis monitoring of Cretaceous submarine basaltic glass during Thellier paleointensity experiments: evidence for alteration and attendant low field bias. Earth Planet. Sci. Lett. 206, 571 585.
Smirnov, A.V., Kulakov, E.V., Foucher, M.S., Bristol, K.E., 2017. Intrinsic paleointensity bias and the long-term history of the geodynamo. Sci. Adv. 3, 7.
Tema, E., Santos, Y., Trindade, R., Hartmann, G.A., Hatakeyama, T., Terra-Nova, F., Matsumoto, N., Mitsumoto, J., Gulmini, M., 2022. Archaeointensity record of weak field recurrence in Japan: new data from Late Yayoi and Kofun ceramic artifacts. Geophys. J. Int. 233, 950 963.
Thellier, É., Thellier, O., 1959. Sur l intensité du champ magnétique terrestre dans le passé historique et géologique. Annales Géophysique 15, 285 376.
Thomas, N., 1993. An integrated rock magnetic approach to the selection or rejection of ancient basalt samples for paleointensity experiments. Phys. Earth Planet. Inter. 75, 329 342.
Wang, H., Kent, D.V., 2013. A paleointensity technique for multidomain igneous rocks. Geochem. Geophys. Geosyst. 14, 4195 4213.
Wang, H., Kent, D.V., 2021. RESET: A Method to Monitor Thermoremanent Alteration in Thellier-Series Paleointensity Experiments. Geophys. Res. Lett. 48, 10.
Wang, H., Kent, D.V., Rochette, P., 2015. Weaker axially dipolar time-averaged paleomagnetic field based on multidomain-corrected paleointensities from Galapagos lavas. Proc. Natl. Acad. Sci. USA 112, 15036 15041.
Wilson, R.L., Watkins, N.D., 1967. Correlation of Petrology and Natural Magnetic Polarity in Columbia Plateau Basalts. Geophys. J. R. Astron. Soc. 12, 405 424.
Xu, S., Dunlop, D.J., 2004. Thellier paleointensity theory and experiments for multidomain grains. J. Geophys. Res. Solid Earth 109, 13.
Yamamoto, Y., Tsunakawa, H., Shibuya, H., 2003. Palaeointensity study of the Hawaiian 1960 lava: implications for possible causes of erroneously high intensities. Geophys. J. Int. 153, 263 276.
Yu, Y., Tauxe, L., 2005. Testing the IZZI protocol of geomagnetic field intensity determination. Geochem. Geophys. Geosyst. 6.
Zhao, X., Liu, Q., Paterson, G.A., Qin, H., Cai, S., Yu, Y., Zhu, R., 2014. The effects of secondary mineral formation on Coe-type paleointensity determinations: Theory and simulation. Geochem. Geophys. Geosyst. 15, 1215 1234.
Zhou, T., Tarduno, J.A., Nimmo, F., Cottrell, R.D., Bono, R.K., Ibanez-Mejia, M., Huang, W., Hamilton, M., Kodama, K., Smirnov, A.V., Crummins, B., Padgett, F., 2022. Early Cambrian renewal of the geodynamo and the origin of inner core structure. Nat. Commun. 13, 7.